ResearchGate

See discussions, stats, and author profiles for this publication at: https://www.researchgate.net/publication/231656145

Magnetic Resonance Imaging of Ruthenium-, Cerium-, and Ferroin-Catalyzed Belousov–Zhabotinsky Reactions

ARTICLE *in* THE JOURNAL OF PHYSICAL CHEMISTRY · JUNE 1996

Impact Factor: 2.78 · DOI: 10.1021/jp953169l

CITATIONS
18

READS
28

3 AUTHORS, INCLUDING:

Albert R Cross
University of Lethbridge
36 PUBLICATIONS **527** CITATIONS
SEE PROFILE

Robin L. Armstrong
University of Toronto
202 PUBLICATIONS **2,814** CITATIONS
SEE PROFILE

Available from: Albert R Cross
Retrieved on: 23 January 2016

Magnetic Resonance Imaging of Ruthenium-, Cerium-, and Ferroin-Catalyzed Belousov−Zhabotinsky Reactions

Ying Gao, Albert R. Cross, and Robin L. Armstrong*

Department of Physics, University of New Brunswick, Fredericton, New Brunswick, Canada E3B 5A3

Received: October 27, 1995; In Final Form: March 7, 1996[⊗]

Magnetic resonance imaging studies of the manganese-catalyzed Belousov−Zhabotinsky (B-Z) reaction have been previously reported. In this paper the results of an investigation of the magnetic relaxation properties of cerium, ruthenium, and iron ions as catalysts for the B-Z system are presented. Criteria are given for the selection of imaging parameters which should yield maximum contrast. Magnetic resonance images of the cerium- and ruthenium-catalyzed B-Z reactions are obtained for the first time. However, the attempt to image the ferroin-catalyzed reaction is unsuccessful. The reason for the failure is identified.

1. Introduction

The Belousov−Zhabotinsky (B-Z) reaction is an extensively studied nonlinear chemical system.[1−3] This reaction involves the oxidation of an organic acid and its brominated form by acidic bromate in the presence of a transition metal ion catalyst. The B-Z reaction is usually catalyzed by Ce(III), Mn(II), Ru(II) {$[Ru(bipy)_3]^{2+}$}, or Fe(II) {$[Fe(phen)_3]^{2+}$}. Spatial chemical waves and patterns associated with this reaction are traditionally detected by optical methods that take advantage of the color change associated with the ionic state of the transition metal ions. The most popular version of the B-Z reaction for study of chemical waves is the Fe(II)-catalyzed reaction.[2,4] In this case a dramatic color change from red to blue accompanies the change from Fe(II) [ferroin] to Fe(III) [ferriin]. Recently, the B-Z reaction catalyzed by Ru(II) has also been reported in pattern formation experiments.[5,6] The photochemical properties of the ruthenium complex have led to new and exciting results in the area of pattern control and manipulation by light.[7−10] This system also exhibits remarkable color contrast.

Magnetic resonance measurements of the Mn(II)-catalyzed, stirred B-Z system were reported by Hansen and Ruoff,[11] and magnetic resonance imaging (MRI) data for the unstirred reaction were first presented by Armstrong et al.[12] In the last few years, MRI has been developed as a powerful means for the visualization and monitoring of chemical waves and patterns[13−18] in this essentially colorless system.

MRI detection of chemical waves associated with the B-Z reaction is based on the contrast of water proton relaxation times (T_1 and T_2) which are determined locally by the presence of the oxidized or reduced state of the catalysts. For the Mn(II)-catalyzed B-Z system, excellent image contrast is achieved because the transverse relaxation time T_2 of the water protons in the system is significantly shorter in the presence of Mn(II) than in the presence of Mn(III).[18] Image contrast based on T_1 differences is also possible, but it is not nearly as good for the Mn(II)-catalyzed system.

MRI detection of traveling plane waves in a narrow tube can be recorded in the form of 1D spatial−temporal graphs as the direct output of the imager.[14] The time required to obtain a single 1D projection is extremely short, less than 10 ms. As a consequence, in setting the timing parameters for optimal contrast, 1D MRI is the place to start since one can wait $5T_1$ between image acquisitions and thereby maximize signal to noise. Even for samples with long T_1 values one can still freeze the motion of the traveling waves since each time-space line is independent of the next.

MRI detection of chemical waves for the B-Z reaction has so far been limited to the Mn-catalyzed system. The current work was undertaken to try to extend the MRI detection of chemical waves to the other B-Z systems, in particular those catalyzed by Ce(III), Ru(II), and ferroin.

The apparatus and experimental procedures are described in section 2. Imaging of the Ce(III)- and Ru(II)-catalyzed B-Z reactions is discussed in section 3. The relaxation times of the oxidized and reduced states of these systems are studied in detail. The results are used to set the parameters in the MRI timing sequence to achieve maximum image contrast. Traveling waves are detected as spatial−temporal graphs. The inversion−recovery imaging technique is used to enhance the contrast. Section 4 is devoted to a consideration of the ferroin-catalyzed B-Z reaction and the special difficulties in imaging it using the MRI technique. A brief summary is given in section 5.

2. Experimental Section

$[Ru(bipy)_3]Cl_2 \cdot 6H_2O$, obtained from the Aldrich Chemical Company, Inc., was converted into the sulfato salt following the procedure of ref 19. The concentration of the stock solution prepared from the sulfato salt was determined spectroscopically. Ferroin solution was prepared in water by mixing ferrous sulfate $FeSO_4$ (98%, Aldrich) and 1,10-phenanthroline (99%, Aldrich) with a ratio of 1:4, to assure no excess of Fe^{2+}. $Ce(SO_4)_2$ (Aldrich), $MnSO_4 \cdot H_2O$ (98.5%, Sigma), and other chemicals were all ACS reagents and used without further purification. Distilled water was used in the experiments.

A Beckman UV−visible spectrophotometer (ACTA CIII) was used to take absorption spectra for determining the concentrations of stock solutions and to carry out the kinetic measurement of the ferroin and ferriin dissociations in acidic solutions.

A TecMag Libra S-16 console acquisition system with a home-built imaging coil (length 80 mm, inner diameter 43 mm) and a Nalorac 2.4 T, 32 cm horizontal-bore, superconducting magnet was used for the relaxation time measurements and the imaging experiments. The magnet is fitted with a set of Nalorac self-shielded gradient coils, 20 cm i.d., which are driven by Techron 7780 amplifiers. The radio frequency amplifier used was a 300 W AMT M3205A.

The ^1H relaxation behaviour of the water in the B-Z systems was investigated by the method[18] of measuring T_1 and T_2

[⊗] Abstract published in *Advance ACS Abstracts,* May 1, 1996.

S0022-3654(95)03169-8 CCC: $12.00 © 1996 American Chemical Society

separately for the oxidized and reduced states of the paramagnetic catalyst ions. An inversion−recovery sequence, with a composite inversion pulse ($90_x-180_y-90_x$), was used for the T_1 measurements, and a CPMG sequence was used for the T_2 determinations. The measurements were carried out in a 1 M sulfuric acid solution at the bore temperature of the magnet (15 ± 1 °C).

Ce(III) stock solution was prepared by adding an excess of malonic acid to a solution of 0.1 M Ce(IV) in 1 M sulfuric acid. The oxidized states of solutions containing Ru(III) and ferriin were obtained by adding an excess of bromate to their respective acidic reduced state solutions. Since ferroin and ferriin are not stable under the experimental conditions, solutions were prepared immediately before the measurements.

The B-Z mixtures were prepared at room temperature by injecting the catalyst into the bulk solution consisting of sulfuric acid, bromate, and malonic acid. The solution was stirred for 1 min before it was transferred into a NMR test tube with an inner diameter of 5 mm and subsequently placed into the spectrometer bore. 1D projection images were taken using the displacement versus time format[16] at the ambient temperature of the magnet (15 ± 1 °C).

The initial concentrations of the mixtures were $[H_2SO_4]$ = 1.25 M, [MA] = 0.15 M, $[BrO_3^-]$ = 0.1 M, and [Ce(IV)] = 0.025 M for cerium as catalyst and $[H_2SO_4]$ = 1 M, [MA] = 0.15 M, $[BrO_3^-]$ = 0.04 M, and [Ru] = 0.010 M for ruthenium.

The 2D images for the Ru-catalyzed B-Z reaction were taken with a circular flat cell (35 mm in diameter and 2 mm thick) using an inversion−recovery FLASH sequence [a 180° pulse followed by 64 low-angle excitation pulses (α = 10°) after a delay near the zero crossing of one state]. The initial concentration of the mixture for 2D imaging was [MA] = 0.09 M, $[BrO_3^-]$ = 0.1 M, $[H_2SO_4]$ = 0.8 M, and [Ru(II)] = 0.0105 M.

In both 1D and 2D imaging experiments, oxygen dissolved in the solutions was not eliminated either before or during the reaction.

3. Imaging the Ce(III)- and Ru(II)-Catalyzed B-Z Reactions

The water proton relaxation times T_1 and T_2 as affected by the presence of Ce(III), Ce(IV), Ru(II), and Ru(III) are plotted in Figure 1 as a function of the ionic concentrations up to their solubility limits. From these data the relationship between relaxation rate, $(1/T_1)$, and paramagnetic ion concentration is confirmed to be linear in each case, as expected.

We see from Figure 1 that the relaxation times are not dramatically shorter than the values for pure water. It follows that imaging of B-Z reactions catalyzed by Ce(III) and Ru(II) will be more difficult than imaging reactions catalyzed by Mn(II).

It is interesting to note that the T_1 and T_2 values for the reduced state of ruthenium are greater than the values for the oxidized state but that the opposite is true for cerium. We can immediately conclude that bright bands on a dark background signifying chemical waves in the one system will be replaced by dark bands on a bright background for the other.

Determination of Timing Parameters for Maximum Contrast. The signal intensity of any pixel obtained using a standard spin-echo imaging sequence is given by

$$M = M_0[1 - e^{-T_R/T_1}]\, e^{-T_E/T_2} \tag{1}$$

where M_0, T_1, and T_2 are the local NMR parameters of the sample at the location of the pixel; T_R is the cycle time for the sequence, and T_E is the time at which the echo occurs as

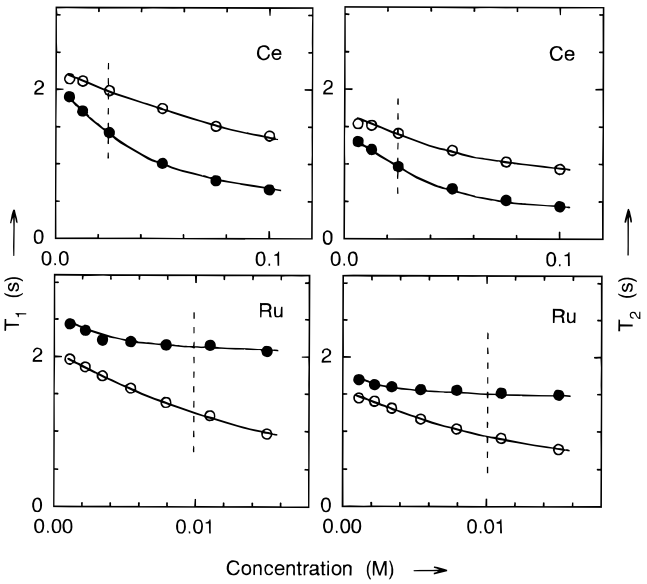

Figure 1. ^{1}H relaxation times T_1 and T_2 as a function of catalyst concentration. The filled circles correspond to the reduced states of the transition metal ions; the open circles correspond to the oxidized states. All the data were measured at 15 ± 1 °C. The solid lines are guides to the eye. The dashed vertical lines indicate the concentrations used for the imaging experiments.

measured from the start of the sequence. The image contrast can be expressed as

$$\frac{\Delta M}{M_0} = \left|\left(\frac{M}{M_0}\right)_a - \left(\frac{M}{M_0}\right)_b\right| \tag{2}$$

where the subscripts *a* and *b* refer to the oxidized and reduced states of the catalyst, or vice versa. Depending on the choice of timing parameters either T_2 weighting or T_1 weighting of the images can be emphasized.

For our discussion of how to choose the timing paramaters it is convenient to deal with the two extreme cases, namely, pure T_2 contrast and pure T_1 contrast. For the former case T_R is set to $5T_1$ or greater; for the latter T_E is set to zero.

For T_2 contrast, $C_2 = \Delta M/M_0$ is given by

$$C_2 = e^{-T_E/T_{2a}} - e^{-T_E/T_{2b}}; \quad T_{2a} \geq T_{2b} \tag{3}$$

Maximum T_2 contrast is obtained when

$$\frac{\partial C_2}{\partial T_E} = -\frac{e^{-T_E/T_{2a}}}{T_{2a}} + \frac{e^{-T_E/T_{2b}}}{T_{2b}} = 0 \tag{4}$$

Therefore, the value of T_E for maximum T_2 contrast is

$$T_{E,max} = \frac{T_{2b}T_{2a}}{T_{2b} - T_{2a}} \ln \frac{T_{2b}}{T_{2a}} \tag{5}$$

Substituting $k_2 = T_{2b}/T_{2a}$ with $0 \leq k_2 \leq 1$ we obtain

$$\frac{T_{E,max}}{T_{2a}} = \frac{k_2}{k_2 - 1} \ln(k_2) \tag{6}$$

It follows that maximum contrast is given by

$$C_{2,max} = k_2^{\,k_2/(1-k_2)} - k_2^{\,1/(1-k_2)} \tag{7}$$

It may easily be shown that the same equations apply to T_1 contrast with T_E replaced by T_R.

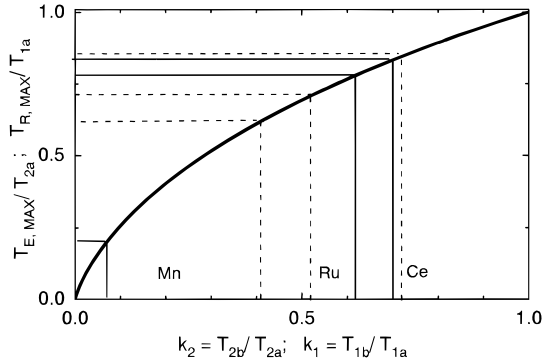

Figure 2. Plot of eq 6 giving T_E/T_{2a} as a function of the ratio of T_2 values, $k_2 = T_{2b}/T_{2a}$. It is also a plot of T_R/T_{1a} as a function of the ratio of T_1 values, $k_1 = T_{1b}/T_{1a}$. The solid lines indicate T_E/T_{2a} values and the dashed lines T_R/T_{1a} values, corresponding to measured k_2 and k_1 ratios for Mn, Ru, and Ce systems. The respective concentrations are [Mn] = 0.001 M, [Ru] = 0.010 M, and [Ce] = 0.025 M.

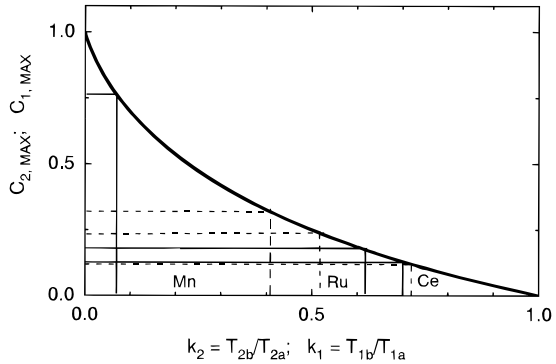

Figure 3. Plot of eq 7 giving $C_{2,max}$, the maximum T_2 contrast, as a function of $k_2 = T_{2b}/T_{2a}$. It is also a plot of $C_{1,max}$ as a function of k_1. The solid lines indicate $C_{2,max}$ values and the dashed lines $C_{1,max}$ values for the same k_2 and k_1 values used in Figure 2.

Figure 2 is a plot of eq 6. It gives the value of T_E/T_{2a} as a function of the ratio of T_2 values, $k_2 = T_{2b}/T_{2a}$. This is also a plot of T_R/T_{1a} as a function of the ratio of T_1 values, $k_1 = T_{1b}/T_{1a}$. The solid lines indicate T_E/T_{2a} values and the dashed lines T_R/T_{1a} values, corresponding to measured k_2 and k_1 ratios for the Mn, Ru, and Ce systems. The respective concentrations are [Mn] = 0.001 M, [Ru] = 0.010 M, and [Ce] = 0.025M.

Figure 3 is a plot of maximum T_2 contrast, $C_{2,max}$, as a function of $k_2 = T_{2b}/T_{2a}$ calculated from eq 7. It is also a plot of maximum T_1 contrast, $C_{1,max}$, as a function of $k_1 = T_{1b}/T_{1a}$. The solid lines indicate $C_{2,max}$ values and the dashed lines $C_{1,max}$ values for the same k_2 and k_1 values chosen in Figure 2 as representative of the Mn, Ru, and Ce systems. Note that maximum contrast is attained only if the proper values of T_E or T_R are selected, as indicated in Figure 2.

Image Acquisition. MRI contrast is determined by the ratio of relaxation times of the reduced and oxidized states of the paramagnetic ions. Figure 1 suggests that the contrast should improve as the concentrations of ruthenium and cerium are increased. Careful scrutiny of this figure also reveals that better contrast is to be expected for the Ru(II)-catalyzed system than for the Ce(III)-catalyzed system. This conclusion is more clearly illustrated in Figure 4, which is a plot of T_2 as a function of time for solutions containing Ce(III), Ce(IV), Ru(II), and Ru(III) concentrations as chosen for the mixtures used in the imaging experiments. We see that the ratio of the T_2 values T_2[Ru(III)]/T_2[Ru(II)] is significantly smaller than the ratio T_2[Ce(III)]/T_2-[Ce(IV)]. This fact is directly related to the prediction that the contrast for the Ru(II)-catalyzed system will be better than the contrast for the Ce(III)-catalyzed system. Figure 4 also shows

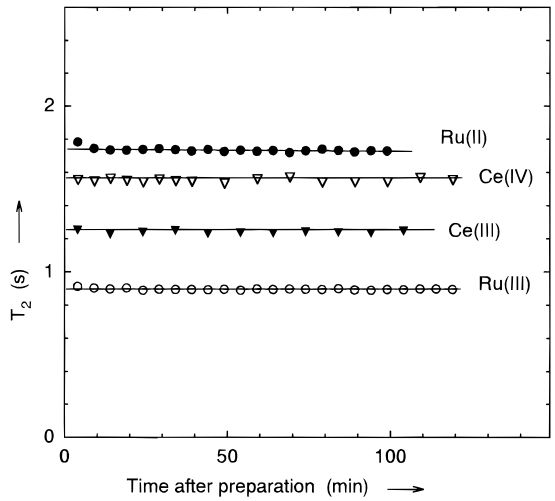

Figure 4. ^{1}H relaxation time T_2 as a function of time after preparation for solutions containing Ce(III), Ce(IV), Ru(II), and Ru(III). The concentration of Ru is 9 mM, and that of Ce is 25 mM.

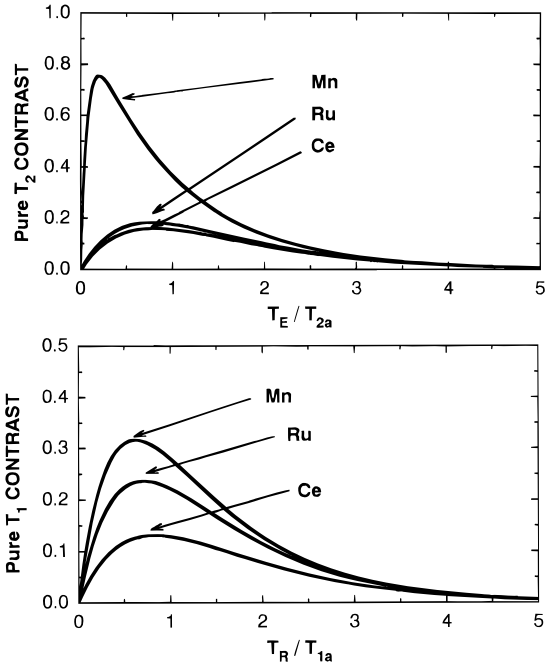

Figure 5. (a, top) Plot of T_2 contrast for Mn(II)-, Ru(II)-, and Ce(III)-catalyzed B-Z mixtures as a function of T_E/T_{2a}. (b, bottom) Plot of T_1 contrast for the same mixtures as a function of T_R/T_{1a}. The concentrations are [Mn] = 0.001 M, [Ru] = 0.010 M, and [Ce] = 0.025 M. Note that the maxima are in the positions predicted by Figures 2 and 3.

that T_2 values are independent of time, which indicates the stability of the ion concentrations. Because of this stability, the relaxation times measured separately for the oxidized and reduced states can be reliably used to set the timing parameters for the imaging sequence to achieve optimum contrast in the resultant images.

Figure 5a shows a comparison of the predicted pure T_2 contrast for Mn(II)-, Ru(II)-, and Ce(III)-catalyzed reactions as a function of T_E/T_{2a}; Figure 5b is a plot of T_1 contrast as a function of T_R/T_{1a} for the same mixtures. The simulations assumed the following metal-ion catalyst concentrations: [Mn] = 0.001 M, [$P_2O_7^{4-}$] = 80 mM, [Ru] = 0.010 M, and [Ce] = 0.025 M. The contrast maxima in each case occur at the T_E and T_R values indicated in Figure 2, and the contrast maxima have the values indicated in Figure 3. The figure illustrates that the best contrast is to be expected for the Mn(II)-catalyzed

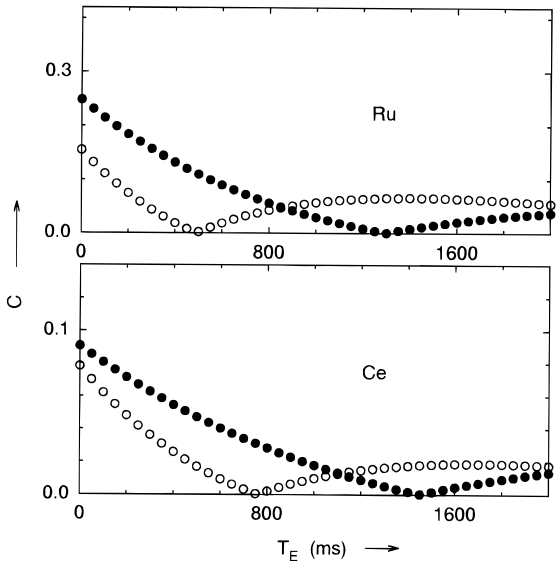

Figure 6. Calculated MRI signal contrast ($C = |\Delta M/M_0|$) versus T_E. The open circles are calculated using eqs 1 and 2 and the filled circles employing eqs 2 and 8. T_R and T_I parameters used for the calculations are set to the same values as used in the experiments.

reaction, followed by the Ru(II)- and Ce(III)-catalyzed reactions. It also shows that T_2 weighting will give the best contrast for Mn(II), whereas T_1 weighting will be best for Ru(II). For Ce(III), T_1 and T_2 contrast are predicted to be about the same.

T_1 contrast may be enhanced by using an inversion−recovery preparation sequence before imaging. In this case eq 1 is modified to become

$$M = M_0[1 - 2e^{-T_I/T_1} + e^{-T_R/T_1}]\, e^{-T_E/T_2} \qquad (8)$$

where T_I is the inversion time. The predicted image contrasts for Ce(III)- and Ru(II)-catalyzed B-Z systems with the concentrations referred to above, a T_R value of 3200 ms, and a T_I value of 1200 ms are calculated according to eqs 1, 2, and 8 and are plotted in Figure 6 as a function of T_E for values up to 2000 ms. The curves with open circles are obtained from calculations using eqs 1 and 2, and the curves with filled circles are from calculations with eqs 2 and 8. The predicted spin−echo image contrasts are in each case poor and get progressively worse as T_E is increased. By using the inversion−recovery technique, some improvement is predicted. For short T_E, the contrast of the Ru(II)-catalyzed system is seen to be increased by more than 50%; and for the Ce(III)-catalyzed system by 10%.

The imaging experiments were performed under the same conditions as used for the simulations. Using the inversion−recovery spin−echo sequence we were able to obtain 1D spatial−temporal plots of traveling waves for both the Ce(III)- and Ru(II)-catalyzed B-Z reactions. Parts a and b of Figure 7 are the displacement versus time images obtained for the Ce(III)- and Ru(II)-catalyzed B-Z reactions, respectively. Figure 7a shows typical trigger waves with a velocity of 2.8 mm/min. Figure 7b illustrates what appears to be a mixture of a trigger wave and a phase wave.[17] In each case the acquisition was started 12 min after preparing the solution. The total repetition time, T_R, was set to 3200 ms, and the T_E values were 15 and 25 ms, for cerium and ruthenium, respectively. The inversion time, T_I, was chosen at 1200 ms to substantially reduce the MR signals from Ce(IV) and Ru(II). Therefore in image 7a the bright background is associated with an excess of Ce^{3+} ions and the dark bands are associated with an excess of Ce^{4+} ions. Similarly, for image 7b, the dark background is related to an excess of Ru(II) and the bright bands are due to an excess of

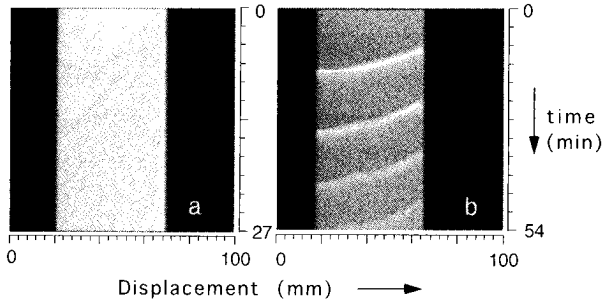

Figure 7. 1D displacement versus time profiles of traveling waves acquired from (a) Ce(III)-catalyzed and (b) Ru(II)-catalyzed B-Z reaction systems. The images of a 5 mm i.d. NMR test tubes containing the B-Z mixtures were taken using a *y*-profile inversion−recovery spin−echo sequence. The parameters used were $T_R = 3200$ ms, $T_I = 1200$ ms for both systems, and $T_E = 15$ ms for Ce(III) and 25 ms for Ru(II). The initial concentrations of the B-Z mixtures are, for cerium, $[H_2SO_4] = 1.25$ M, $[MA] = 0.15$ M, $[BrO_3^-] = 0.1$ M, and $[Ce(IV)] = 0.025$ M; for ruthenium, $[H_2SO_4] = 1$ M, $[MA] = 0.15$ M, $[BrO_3^-] = 0.04$ M, and $[Ru(II)] = 0.01$ M.

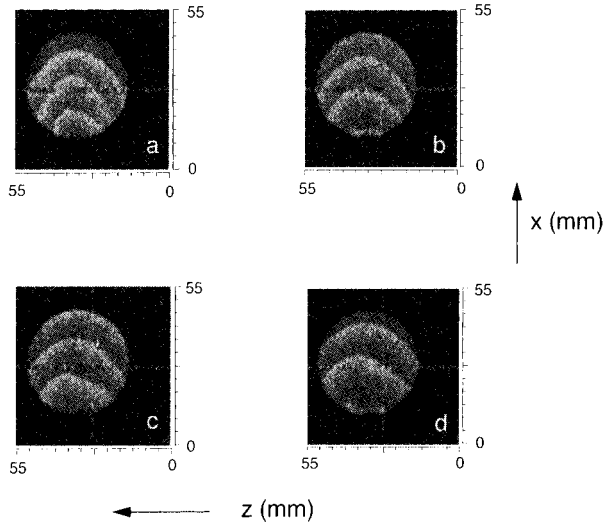

Figure 8. 2D images of chemical waves in the Ru(II)-catalyzed B-Z reaction. The first image was taken 5 min after the preparation with a flat circular glass cell (35 mm in diameter and 2 mm thick). Successive pictures were taken at 2 min intervals. The initial concentrations of the components are $[MA] = 0.09$ M, $[BrO_3^-] = 0.1$ M, $[H_2SO_4] = 0.8$ M, and $[Ru(II)] = 10.5$ mM. The waves are propagating from the neck of the cell (bottom of the picture).

Ru(III). The contrast for the Ru(II)-catalyzed system is better by at least a factor of 3 than that for the Ce(III)-catalyzed system. Both aspects of the behavior are as predicted for the inversion−recovery spin−echo sequence.

In addition, 2D images of chemical waves in the Ru(II)-catalyzed B-Z system were acquired successfully by applying an inversion−recovery FLASH sequence. With the standard spin−echo imaging sequence, the total acquisition time would be $1.6\ \text{s} \times 128 = 3.4$ min. This is too long for waves traveling at about 3 mm/min. Fast imaging techniques employ low flip angle pulses and exhibit lower T_1 contrast. The total acquisition time is reduced to about 10 s. The combination of an inversion−recovery preparation with a FLASH sequence maintains the T_1 contrast. The reaction was first initiated using bromate in a batch reactor, and then the mixture was transferred into a circular flat cell which was immediately placed horizontally in the magnet. The cell has a diameter of 35 mm and a thickness of 2 mm. Figure 8 depicts successive images taken at 2 min intervals. The first acquisition was taken 11 min after the start of the reaction. The inversion time was set to 1.6 s to significantly reduce the signal from Ru(II). It is seen that the

contrast is quite reasonable. The figure depicts a circular wave disturbance emanating from a pacemaker with a period of about 4 min located at the neck of the cell (bottom of picture) and propagating with a speed of 4.2 mm/min.

However, it was not possible to obtain such images for the Ce(III)-catalyzed B-Z reaction because of the poorer contrast as predicted on the basis of the measurement of the relaxation times and the fact that the flash sequence produces results which are always noisier than optimal.

4. Imaging the Ferroin-Catalyzed B-Z Reaction

Imaging chemical waves of the ferroin/ferriin B-Z reaction turned out to be impossible. The waves readily observable by eye could not be visualized with the MRI spectrometer using either the spin-echo sequence or the inversion−recovery spin−echo sequence.

The observed water proton relaxation times in the reduced and oxidized states were found to be temperature dependent and to decrease with time. Figure 9 shows the T_2 values for ferroin and ferriin for a particular mixture at 20 °C as a function of time. In both cases T_2 decreases with time, but much more rapidly for ferriin than ferroin. This suggests that T_2 contrast should improve significantly with time. The fact that it does not indicates that whatever is causing the T_2 of ferriin to decrease must not be active in the B-Z oscillation.

It is known that ferroin is unstable in acidic solutions and that it dissociates slowly to give ferrous ions, Fe^{2+}, and the protonated form of 1,10-phenanthroline (phen).[20]

$$[Fe(phen)_3]^{2+} + 3H^+ \rightleftharpoons Fe^{2+} + 3phenH^+$$

In the B-Z reaction system, ferrous ions released by the dissociation can be easily oxidized to ferric ions.

$$Fe^{2+} + [O] \rightarrow Fe^{3+}$$

where [O] means any oxidants present in the system.

Ferriin is also unstable; it dissociates to release ferric ions.[21]

$$[Fe(phen)_3]^{3+} \rightarrow Fe^{3+} + 3phen$$

In the presence of ferrous ions, ferriin can be converted to ferric ion very rapidly through the reaction.[21]

$$[Fe(phen)_3]^{3+} + Fe^{2+} \rightarrow [Fe(phen)_3]^{2+} + Fe^{3+}$$

The decay of ferriin was checked spectrophotometrically in the B-Z media ($[BrO_3^-] = 0.05$ M and $[H_2SO_4] = 0.17$, 1, and 3 M). We also followed the ferroin dissociation, but only in 1 M sulfuric acid because this reaction is independent of acidity.[20,21] The absorbance decay was monitored at room temperature with a 1 cm path length optical cell at a wavelength of 600 nm for ferriin and 510 nm for ferroin. The concentration decays of ferroin and ferriin were calculated from the measured absorbances and found to agree with previous results.[21] It may be concluded that ferroin and ferriin solutions are both unstable in the acidity range of the B-Z reaction. As a result, ferric ions can be continuously released and accumulated through the dissociation of both ferroin and ferriin.

We measured the relaxation times T_1 and T_2 in solutions containing ferric (Fe^{3+}) ions. For a specific concentration of Fe^{3+} ions, equivalent relaxation times occur for a ferriin solution with a concentration 10 times greater. For example, for a 1 mM concentration of Fe^{3+} ions, $T_1 = 70$ ms and $T_2 = 43$ ms; these values roughly correspond to those for a 10 mM ferriin solution. This is the explanation of the dramatic decay of the T_2 of ferriin with time as seen in Figure 9. Within 20 min enough ferric ions have been produced to dominate the relaxation times.

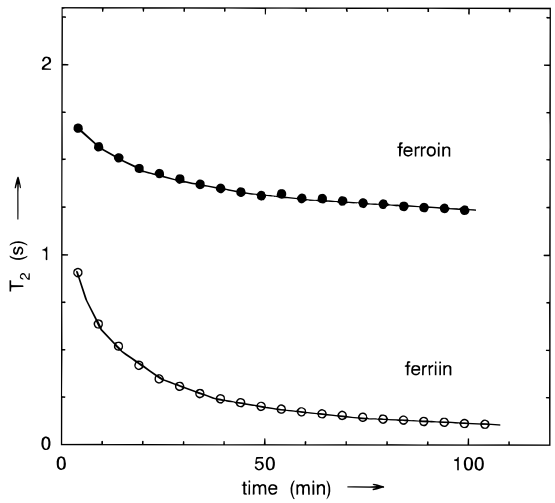

Figure 9. ^1H relaxation time T_1 as a function of time after the preparation of ferroin and ferriin solutions in 1 M H_2SO_4. The initial concentrations of ferroin and ferriin are 7 mM.

It is now understandable why we were unable to observe chemical waves in the ferroin-catalyzed B-Z reaction. As a consequence of the instability of ferriin, and the associated production of ferrous and ferric ions, the local proton relaxation times do not provide an indicator of the presence of chemical wave activity.

5. Conclusion

The results of this work demonstrate the capability of the MRI technique for the detection of chemical waves associated with the Belousov−Zhabotinsky reactions catalyzed by Ce(III) and Ru(II). Relaxation time measurements indicate that the contrast should improve with increasing concentration. Both 1D and 2D images with good contrast were obtained for the Ru(II)-catalyzed system. For the Ce(III)-catalyzed reaction, a 1D image, with poorer contrast, was obtained. No success was achieved in the 2D imaging experiment.

The inability of MRI for visualizing chemical waves in the ferroin-catalyzed B-Z reaction was shown to be due to the existence of ferric ions which are formed and accumulated as the final product of both ferroin and ferriin decompositions. Local differences in proton relaxation times, needed for MRI detection, quickly become dominated by the presence of ferric ions, making all regions of space appear with the same intensity.

The inversion−recovery spin−echo technique is shown to be effective and useful to improve the imaging sensitivity for systems with long relaxation times. The success in detecting chemical waves of Ru(II)- and Ce(III)-catalyzed B-Z reactions illustrates a possibility of extending the application of the MRI technique to other nonlinear dynamic systems.

Acknowledgment. The research was funded in part by a grant to R.L.A. from the Natural Science and Engineering Research Council of Canada.

References and Notes

(1) Zhabotinsky, A. M. *Dokl. Akad. Nauk SSSR* **1964**, *157*, 392.
(2) *Oscillations and Travelling Waves in Chemical Systems*; Field, R. J., Burger, M., Eds.; Wiley-Interscience: New York, 1985.
(3) Field, R. J.; Körös, E.; Noyes, R. M. *J. Am. Chem. Soc.* **1972**, *94*, 8649.
(4) Winfree, A. T. *Science* **1973**, *181*, 937.
(5) Kuhnert, L.; Krug, H. J. *J. Phys. Chem.* **1987**, *91*, 730.

(6) Weigt, H. R. *Angew. Chem.* **1992**, *104*, 358.
(7) Kuhnert, L. *Nature* **1986**, *319*, 393.
(8) Markus M.; Nagy-Ungvarai, Zs.; Hess, B. *Science* **1992**, *257*, 225.
(9) Steinbock, O.; Muller, S. C. *Physica A* ***1992***, *188*, 61.
(10) Reddy, R.; Nagy-Ungvarai, Zs.; Muller, S. C. *J. Phys. Chem.* **1994**, *98*, 12255.
(11) Hansen, E. W.; Ruoff, P. *J. Phys. Chem.* **1989**, *93*, 264.
(12) Armstrong, R. L.; Tzalmona, A.; Menzinger, M.; Cross, A.; Lemaire, C. Abstracts XXV Congress Ampere, Stuttgart, FDR, 1990; pp 94−95.
(13) Tzalmona, A.; Armstrong, R. L.; Menzinger, M.; Cross, A.; Lemaire, C. *Chem. Phys. Lett.* **1990**, *174*, 199.
(14) Tzalmona, A.; Armstrong, R. L.; Menzinger, M.; Cross, A.; Lemaire, C. *Chem. Phys. Lett*. **1992**, *188*, 457.
(15) Menzinger, M.; Tzalmona, A.; Armstrong, R. L.; Cross, A.; Lemaire, C. *J. Phys. Chem*. **1992**, *96*, 4725.
(16) Su, S.; Menzinger, M.; Armstrong, R. L.; Cross, A. R.; Lemaire, C. *J. Phys. Chem.* **1993**, *98*, 7295.
(17) Su, S.; Menzinger, M.; Armstrong, R. L.; Cross, A. R.; Lemaire, C. *J. Phys. Chem.* **1994**, *98*, 2494.
(18) Cross, A. R.; Armstrong, R. L.; Reid, A.; Su, S.; Menzinger, M. *J. Phys. Chem.* **1995**, *99*, 16616.
(19) Gao, Y.; Försterling, H.-D. *J. Phys. Chem*. **1995**, *99*, 8638.
(20) Brandt, W. W.; Dwyer, F. P.; Gyarfas, E. C. *Chem. Rev.* **1959**, ***54***, 959.
(21) Chou, Y.-C.; Lin, H.-P.; Sun, S. S.; Jow, J.-J. *J. Phys. Chem*. **1993**, *97*, 8450

JP953169L